P4.1 SEA-BREEZE CASE STUDY USING A COMBINATION OF OBSERVATIONAL AND NUMERICAL SIMULATION IN COMPLEX TERRAIN IN SOUTHERN FRANCE: CONTRIBUTION TO MATTER TRANSPORT;

S. Bastin[1,*], P. Drobinski[1], A.M. Dabas[2], P. Delville[3], O. Reitebuch[4], C. Werner[4]
(1) IPSL/SA, Paris, France; (2) CNRM/Météo-France, Toulouse, France; (3) DT-INSU, Meudon, France; (4) DLR, Wessling, Germany;

1*. INTRODUCTION

Sea breeze dynamics in the Marseille area, in southern France, is investigated in the framework of the ESCOMPTE experiment (field experiment to constrain models of atmospheric pollution and emissions transport; Cros et al., 2004) conducted during summer 2001 in order to evaluate the role of thermal circulations on pollutant transport and ventilation. The topography of the surroundings is complex (see Fig.1 et 2) with the presence of the Mediterranean sea and two mountain barriers of different heights separated by the Rhone valley, a gap of 200 km long and 60 km width. This topography suggests that processes described by several authors (for example, Lu and Turco, 1994), inducing both sea breeze circulations, slope flows and valley flows are likely to occur and interact together to generate different air polluted layers in a wide domain around Marseille. Anymore, Fig.1 shows that the coastal shape is not linear and becomes a regional feature to be accounted for in the alteration of the sea breeze (Gilliam et al., 2003). The aim of this paper is to identify the main mecanisms that transport pollutants rejected near the coastline by the large city of Marseille and its industrialized suburbs (Fos-Berre area). The objectives of the paper are adressed using both the dataset collected during the 25 June 2001 ESCOMPTE case (hereafter called J25) and a numerical simulation that was completed with the french non hydrostatic mesoscale model, Meso-NH. This study reveals that three major processes contribute to the transport of matter: the advection of pollutants inland is mainly driven by two breeze cells that occur on two different depth and time scales, and vertical exchanges between the atmopsheric boundary layer and the free troposhere can be generated at the breeze front and near the slopes due to the development of anabatic winds. The horizontal and vertical mass fluxes are quantitatively evaluated thanks to the numerical simulation.

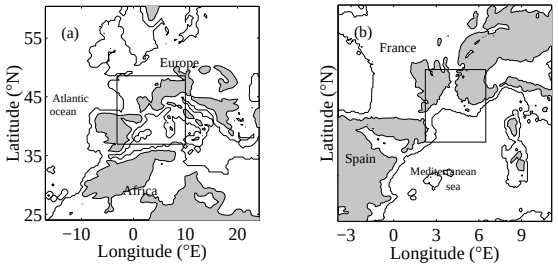

Figure 1: (a) Map of the coarsest domain of the simulation with its nested smaller domain (domain 2) in the rectangle. The topography is shaded in grey when higher than 500 m.. (b) Domain 2 with its nested smaller domain (domain 3) in the rectangle.

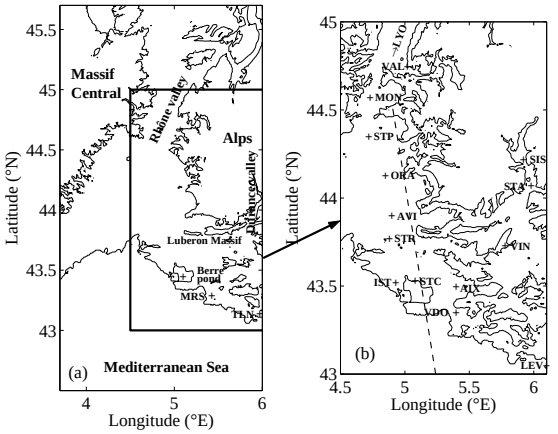

Figure 2: (a) Domain 3 of the simulation. (b) Zoom of the target area. Acronyms are for Istres (IST), Saint Remy (STR), Avignon (AVI), Orange (ORA), Saint Paul (STP), Montélimar (MON), Vallon d'Ol (VDO). The dashed line indicates the flight track of the DLR Falcon 20 carrying the Doppler lidar WIND on 25 June 2001.

2. MEASUREMENTS AND MODEL

2.1 Instrumental set-up.

A wide range of instruments was deployed around Marseille, leading to a dense network of observations (see the details in Cros et al., 2004). In this study, we will mainly make use of the data derived from the operational meteorological surface station network, from the airborne Doppler lidar WIND (Werner et al, 2001), from the RASS sodar

* *Corresponding author address:* Sophie Bastin, Service d'Aéronomie, Université Pierre et Marie Curie, Tour 45, 4, Place Jussieu, 75252 Paris Cedex 05, France.
e-mail: sophie.bastin@aero.jussieu.fr

located at Vallon d'Ol (see Fig.2), and radiosoundings at StRémy and Nimes.

2.2 Model description

The numerical simulation was conducted with the model Meso-NH that solves the non-hydrostatic and anelastic equation system (Lafore et al., 1998). A 24-hr simulation initialized at 00 UTC on J25 was completed using stationary 2-km and 8-km resolution domains nested within a 40-km domain using two-way interfaces. The three domain are represented on Figs 1 and 2. The initial and coupling fields were generated by first interpolating the analysis data of the European Center available every 6 hours on a 0.25° x 0.25° latitude-longitude grid to the model grid. The vertical grid is made of 50 levels with a mesh streched between 60 and 600 m. To insure a good description of the atmospheric boundary layer, 12 levels are taken below 1000 m. A complete sets of physics parametrization is used.

3. FLOW EVOLUTION AND STRUCTURE

The synoptic situation on J25 is propitious to the development of a sea breeze circulation with high pressure at the surface and no significant pressure gradient at 850 hPa. A moderate northerly flow induced by topography blows in the lower layer of the atmosphere in the Rhône valley. This offshore wind and the sea breeze flow have a close speed but nearly opposite directions. The two wind systems might collide and generate a front. The structure of this front is discussed in next sections.

3.1 Spatial and temporal evolution of the sea breeze near the surface.

Figure 3 shows a horizontal cross section of the observed and the simulated surface temperature in the Rhône valley along the line IST, STR, AVI, ORA, STP, MON at four different times on J25 (0800, 1300, 1600 and 1800 UTC). The point at latitude 43.5°N corresponds with the sea surface temperature (SST). The observed SST (20.7°C) is derived from NOAA observations. This figure shows that a temperature gradient exists between the sea and the land for the four times but the location of the maximum surface temperature evolves during the day. The measurements indicate that the maximum is very close to the coastline at 0800 UTC and it progressively moves inland. This suggests that the breeze cell progressively extends inland as predicted by theory. The model results show the same general evolution of the surface temperature, even though at 0800 UTC, the surface temperature is lightly overestimated by the model in the Rhône valley (2 to 3°C). From 1300 UTC, the difference in temperature is totaly reduced and the model results and observations are in very good agreement.

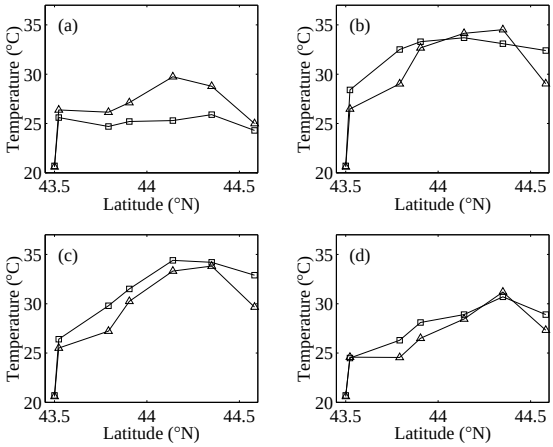

Figure 3: *Horizontal cross section of the observed (squares) and simulated (triangles) surface temperature along the line IST, STR, AVI, ORA, STP, MON (see Fig.2) on J25 at 0800 (panel a), 1100 (panel b), 1300 (panel c) and 1600 UTC (panel d). The observed temperature is derived from the meteorological surface station network of Météo-France.*

Figure 4 displays the wind speed and direction at Istres, Avignon and Orange from both the numerical simulation (triangles) and observations (squares). It shows that in the morning, as the radiational heating increases over land, inducing the increase of the surface temperature (Fig. 3), the sea breeze intensifies and extends inland. Measurements indicate that the sea breeze already blows at Istres at 0800 UTC and it reaches Avignon at about this time, even though the wind is very weak leading to strong uncertainty on the wind direction. The wind at Avignon strengthens at about 1300 UTC. The breeze flow reaches Orange at 1600 UTC. This evolution can easily be explained by the surface temperature. A good correlation is observed between Figs 3 and 4: as the radiational heating increases, the temperature surface increases (Fig 3a et 3b). This generates a temperature gradient that induces the onset of the breeze flow near the coastline (Figs 4a; b; c and d). As the sea breeze propagates inland and intensifies, the surface temperature decreases due to the advection of cooler air over land and the maximum of temperature moves landward (Figs 3 c and d). Then, the sea breeze propagtes further inland and reaches Orange (Figs 4e and 4f).

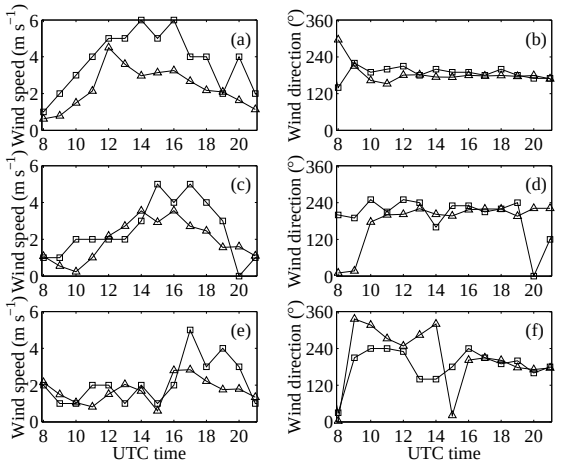

Figure 4: Temporal evolution of the wind speed (left side) and wind direction (right side) at Istres (panels a and b), Avignon (panels c and d) and Orange (panels e and f). Squares stand for measurements and triangles stand for model results

Good agreements are found with the model except that the wind speed is lightly underestimated (up to 3 m s^{-1}), while the temperature gradient driving the breeze flow is well estimated. It may be due to the influence of the synoptic wind that is not well simualted by the model (see after).

3.2 Shallow and deep sea breezes

The comparisons between vertical profiles of the wind speed and direction derived from the model results and the observations from radiosoundings launched from Saint Rémy and Nimes (not shown) show very good agreement in the lower layer (from the ground up to 2000 m) and higher than 4000 m but they show an important bias of the wind speed (about 5.m s^{-1}) in the layer between 2000 and 4000 m.

The vertical structure of the wind in the lower layer near the coastline shows evidence of the existence of two sea breezes driven by two scales of temperature contrast Banta, 1995): (i) a local temperature gradient that is maximum in the direction normal to the ocastline; (ii) a mesoscale temperature gradient between the cold waters offshore and the hot surface temperatures of the interior of the Rhône valley. Indeed, Figure 5 displays the horizontal wind vectors along the coastline at 60 m above ground level (AGL) (panel a) and at 500 m above sea level (ASL) (panel b) at 1300 UTC. It clearly shows that, near the surface, the direction of the wind is strongly influenced by the coastline shape which is consistent with previous observational studies in other areas (Physick and Byron-Scott, 1977). On the contrary, at 500 m ASL, the direction of the breeze is more homogeneous.

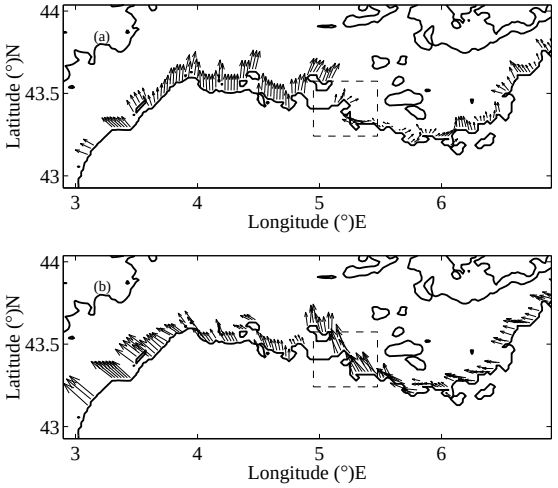

Figure 5: Horizontal wind along the coastline near the surface (a) and at 500 m above sea level (b). The rectangle in dashed line displays the smaller area where the sodar was located.

A sodar was located at Vallon d'Ol, in the northern suburbs of Marseille (see the thick cross on Fig.5), at 280 m ASL. Observations retrieved from this sodar show that the wind direction near the surface is oriented southwesterly and it progressively turns southwards (Fig.6).

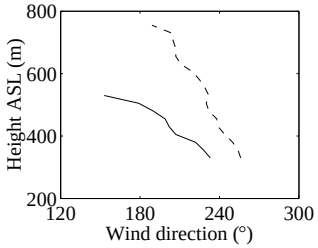

Figure 6: Wind direction at 1100 (solid line) and 1600 UTC (dashed line) as derived from sodar data at Vallon d'Ol.

We use the simulation to complete sodar observations. The model results are in agreement with these observations. Indeed, Figure 7 displays vertical profiles of the wind speed and direction at three different but close locations at 1100 (panels a and b) and 1600 UTC (panels c and d) respectively. These locations are indicated on Fig.8 by the same symbol as those used for the vertical profile. The orientation of the coastline is different for each of the locations. Figure.7 shows that near the surface, the wind direction is nearly normal to the coastline. Thus, the three profiles are disjoined near the surface. While the altitude increases, the wind turns progressively to converge on a unique direction that is about 150° at 1100 UTC and 180° at 1600 UTC.

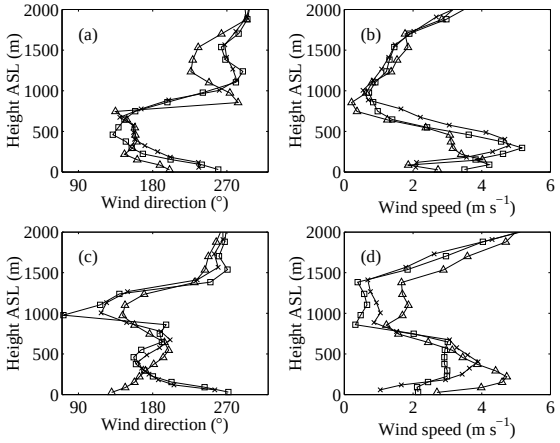

Figure 7: Wind direction (left panels) and wind speed (right panels) at the three locations indicated on Fig.\ref{coast} as derived from the model outputs at 1100 (panels a and b) and 1600~UTC (panels c and d).

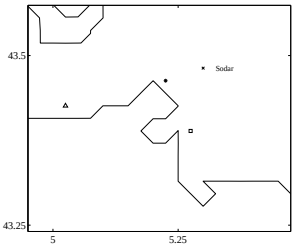

Figure 8: zoom of the topography near Marseille. The thick cross indicates the location of the sodar at Vallon d'Ol. The triangle, star and square indicate the locations where vertical profiles of the wind are extracted from the simulation.

3.3 The breeze front

Figure 9 shows a comparison between the vertical cross section of the horizontal wind measured by the Doppler lidar WIND along the leg indicated on Fig.2 in dashed line at about 1700 UTC and the same vertical cross.section as derived from the model output at 1600 UTC. Arrows indicate the direction of the horizontal wind and color is for the wind speed. A good colocation of the convergence zone between lidar observations and model outputs is observed but with a delay. This figure also confirms that bad agreements are found between observations and simulation in the layer between 1 and 2 km ASL.

Other vertical cross sections (not shown) indicate that the sea breeze front is maximum in intensity at about 1400 UTC, showing strong updraft with a magnitude of 1 m s^{-1} in the frontal region at a height of 800 m AGL. The major contribution to the TKE budget is shear production. After 1400 UT, the breeze front propagates inland while the magnitude of the updraft decreases.

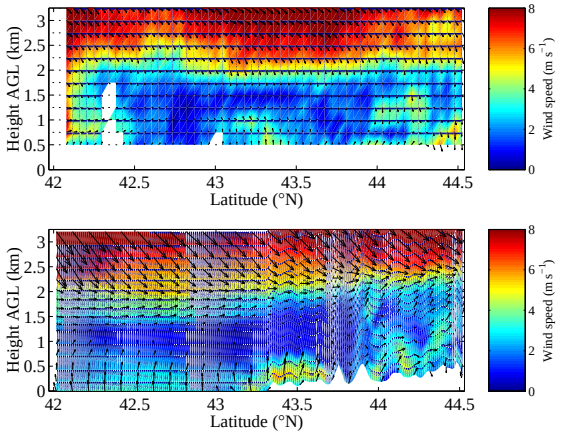

Figure 9: Vertical cross section of the horizontal wind along the leg indicated on Fig.2 in dashed line. Arrows indicate the direction of the horizontal wind and color is for the wind speed.

.

4. MASS TRANSPORT

The previous section has shown the complexity of the mesoscale circulation in such an area. Several mechanisms have been described that could impact on the pollutants transport. To quantify this mass transport, we divise the target area into several boxes and we compute the mass fluxes for all the sides of each box by:

$$\begin{cases} \rho\bar{u} = \int_{x_{\min}}^{x_{\max}} dx \int_{z_1}^{z_2} \rho(x,z)u(x,z)dz \\ \rho\bar{w} = \int_{x_{\min}}^{x_{\max}} dx \int_{y_{\min}}^{y_{\max}} \rho(x,y,z_2)w(x,y,z_2)dy \end{cases}$$

where ρ is the air density, u is the component of the wind normal to the integration surface, w is the vertical velocity, z_1 and z_2 are two different vertical levels that will be defined after and x_{min}, x_{max}, y_{min} and y_{max} delimit boxes of 20 km * 20 km. Figure 10 represents mass fluxes across the different faces of boxes between the ground and 300 m ASL (a), and between 300 and 1000 m ASL (b) on J25 at 14 and 18 UTC. At 09 UTC, a positif vertical mass flux is visible along the 500 m isocontour of the topography due to the onset of upslope winds. At this time, the horizontal advection of mass due to the sea breeze is not visible. The horizontal mass flux integrated between the surface and 300 m ASL is weak, in agreement with surface stations that show no well marked wind direction in the target area. Between 300 and 1000 m, some matter is advected from the north. In the southwesterly part of the target area, matter goes westwards due to the synoptic situation that shows a shallow depression above Spain. At 1000 UTC,

upslope winds reinforce inducing an increase of the vertical transport up to 1000m. The advection by the sea breeze flow becomes significant from 1100 UTC. In the lower part, this advection reaches 30 km from the coastline. But it is still not visible in the second layer even if the transport induced by the northerly flow is quasi cancelled when approaching the shoreline. The vertical mass transport induced by the breeze front presents spatial inhomogeneities. The matter is lofted in the second layer but the breeze front is not strong enough to fill the troposphere higher than 1000 m with matter from the surface. At 1400 UTC (Fig 10a), the horizontal advection of mass by the sea breeze is really efficient. Quantitatively, it is nearly the same in the two layers. The feeding of boxes by meridian fluxes is compensated by vertical fluxes (induced by the breeze front at the middle of the Rhône valley and by upslope winds) and by zonal fluxes specially near the slopes. At this time, the vertical transport is stronger near the slopes than in the middle of the Rhône valley. In the south-eastern part of the target area, a convergence zone appears and create strong vertical mass fluxes. At 1800 UTC (Fig. 10b), all the mass fluxes have decreased. The breeze front penetrates further inland, beyond 44.5°N. The vertical transport is important along the line oriented west-east that represents the limit of the breeze flow, especially along the slope, which confirms that the interactions between sea breeze and heated-mountain flows can intensify and acelerate upslope flows.

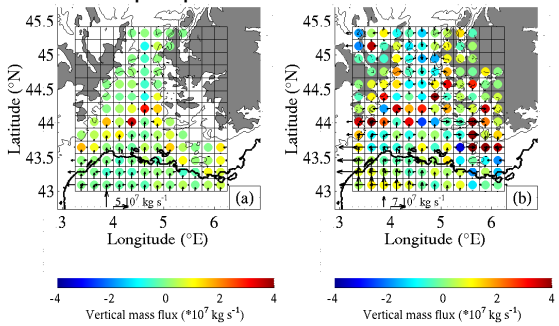

Figure 10: Horizontal and vertical mass fluxes calculated from Méso-NH at 1400 UTC.. Arrows are fit within the importance of the horizontal mass flux and indicate its direction. Color represents the sign and the importance of the vertical mass flux.

5. CONCLUSION

This study shows that the complex topography of the target area induces several circulations at local and mesoscale. This study reveals that three major processes contribute to the transport of matter: the advection of pollutants inland is mainly driven by two breeze cells that occur on two different depth and time scales, and vertical exchanges between the atmopsheric boundary layer and the free troposhere can be generated at the breeze front and near the slopes due to the development of anabatic winds. The impact of upslope flows seems to be more important than the impact of the breeze front.

6. REFERENCES

Cros et al., 2004: `The ESCOMPTE Program: An Overview', Atmos. Res., in press.

Gilliam, R.C., Raman, S., Niyogi, D.D.S., 2004: Observational and numerical study on the influence of large-scale flow direction and coastline shape on sea-breeze evolution. *Bound.-Lay. Meteorol.*, **111**, 275-300.

Lafore et al., 1998: The Méso-NH atmospheric simulation system. Part I: Adiabatic formulation and control simulation. *Ann. Geophys.*, **16**, 90-109.

Lu, R., and Turco, R.P., 1994: Air pollutant transport in a coastal environment. Part I: Two-dimensional simulations of sea-breeze and mountain effects. *J. Atmos. Sci.*, **51**, 2285-2308.

Physick, W.L., Byron-Scott, R.A.D., 1977: Observations of the sea-breeze in the vicinity of a gulf. *Weather,* **32**, 373-381

Werner, C., P.H. Flamant, O. Reitebuch, F. Köpp, J. Streicher, S. Rahm, E. Nagel, M. Klier, H. Herrmann, C. Loth, P. Delville, P. Drobinski, B. Romand, C. Boitel, D. Oh, M. Lopez, M. Meissonnier, D. Bruneau, A.M. Dabas, 2001: Wind Instrument. *Opt. Eng.*, **40**, 115-125.